NeuroImage 210 (2020) 116556

Contents lists available at ScienceDirect

NeuroImage

journal homepage: www.elsevier.com/locate/neuroimage

Comparing MEG and high-density EEG for intrinsic functional connectivity mapping

N. Coquelet [a,*], X. De Tiège [a,b,c], F. Destoky [a], L. Roshchupkina [a,c], M. Bourguignon [a,d,e], S. Goldman [a,b], P. Peigneux [c], V. Wens [a,b]

[a] Laboratoire de Cartographie fonctionnelle du Cerveau, UNI-ULB Neuroscience Institute, Université libre de Bruxelles (ULB), Brussels, Belgium
[b] Magnetoencephalography Unit, Department of Functional Neuroimaging, Service of Nuclear Medicine, CUB Hôpital Erasme, Brussels, Belgium
[c] Neuropsychology and Functional Neuroimaging Research Unit (UR2NF), Centre for Research in Cognition and Neurosciences (CRCN), UNI-ULB Neuroscience Institute, Université libre de Bruxelles (ULB), Brussels, Belgium
[d] Laboratoire Cognition Langage et Développement, UNI-ULB Neuroscience Institute, Université libre de Bruxelles (ULB), Brussels, Belgium
[e] BCBL, Basque Center on Cognition, Brain and Language, 20009, San Sebastian, Spain

ARTICLE INFO

Keywords:
Connectome
State dynamics
Resting-state networks
Envelope correlation
Magnetoencephalography
Electroencephalography

ABSTRACT

Magnetoencephalography (MEG) has been used in conjunction with resting-state functional connectivity (rsFC) based on band-limited power envelope correlation to study the intrinsic human brain network organization into resting-state networks (RSNs). However, the limited availability of current MEG systems hampers the clinical applications of electrophysiological rsFC. Here, we directly compared well-known RSNs as well as the whole-brain rsFC connectome together with its state dynamics, obtained from simultaneously-recorded MEG and high-density scalp electroencephalography (EEG) resting-state data. We also examined the impact of head model precision on EEG rsFC estimation, by comparing results obtained with boundary and finite element head models. Results showed that most RSN topographies obtained with MEG and EEG are similar, except for the fronto-parietal network. At the connectome level, sensitivity was lower to frontal rsFC and higher to parieto-occipital rsFC with MEG compared to EEG. This was mostly due to inhomogeneity of MEG sensor locations relative to the scalp and significant MEG-EEG differences disappeared when taking relative MEG-EEG sensor locations into account. The default-mode network was the only RSN requiring advanced head modeling in EEG, in which gray and white matter are distinguished. Importantly, comparison of rsFC state dynamics evidenced a poor correspondence between MEG and scalp EEG, suggesting sensitivity to different components of transient neural functional integration. This study therefore shows that the investigation of static rsFC based on the human brain connectome can be performed with scalp EEG in a similar way than with MEG, opening the avenue to widespread clinical applications of rsFC analyses.

1. Introduction

The human brain intrinsically organizes into large-scale functional networks that play a central role in major human brain functions such as the processing of sensory stimuli, goal-directed task performance, or spontaneous cognition (for a review, see, e.g., Deco and Corbetta, 2011). Functional magnetic resonance imaging (fMRI) investigations of resting-state functional connectivity (rsFC) identified several resting-state networks (RSNs) (for a review, see Fox and Raichle, 2007). Similar RSNs were also uncovered using magnetoencephalography (MEG) combined with the band-limited envelope correlation method (Brookes et al., 2011; de Pasquale et al., 2010; Hipp et al., 2012; Wens et al., 2014a; for a review, see also O'Neill et al., 2015a), thereby shedding light on their spectral and temporal dynamics (Brookes et al., 2011; de Pasquale et al., 2010; Hipp et al., 2012; Wens et al., 2019).

The concept of rsFC also bears great clinical interest as it requires minimal patient participation and mitigates biases related to differences in task-related performance (for reviews, see, e.g., Fox, 2018; Fox and Greicius, 2010). A distinct advantage of electrophysiological rsFC is to avoid the issue of altered regional neurovascular coupling occurring in several brain disorders (for a review, see D'Esposito et al., 2003) and healthy ageing (Coquelet et al., 2017), that impacts on the fMRI blood

* Corresponding author. Laboratoire de Cartographie fonctionnelle du Cerveau, UNI-ULB Neuroscience Institute, Université libre de Bruxelles (ULB), 808 Lennik Street, 1070, Brussels, Belgium.
E-mail address: ncoquele@ulb.ac.be (N. Coquelet).

https://doi.org/10.1016/j.neuroimage.2020.116556
Received 14 June 2019; Received in revised form 11 December 2019; Accepted 14 January 2020
Available online 20 January 2020

oxygen level dependent signal. Still, widespread translation of MEG-based rsFC from research to clinics is bound to be hampered by the limited availability and cost of current cryogenic MEG systems (notwithstanding the prospects of wearable MEG relying on optically pumped magnetometers, see Boto et al., 2018). On the other hand, electroencephalography (EEG) is considerably cheaper (even in its high-density version) and thus more accessible to clinical environments, motivating the translation of rsFC and RSN mapping from MEG to EEG.

Using simultaneous MEG/EEG recordings, the seminal study of Siems et al. (2016) showed that 64-channel scalp EEG is sufficient to reconstruct (at least) four RSNs similar to those obtained with MEG, albeit with lesser spatial resolution possibly due to a smaller number of sensors. Liu et al. (2017, 2018) were able to detect most of the classical RSNs with better spatial resolution by combining high-density 256-channel scalp EEG and advanced head modeling. Alongside a few others (Knyazev et al., 2016; Sockeel et al., 2016), these studies confirmed the ability of scalp EEG to map classical RSNs as with MEG, and widened the clinical prospects of RSN mapping. Still, topics developed in recent fMRI and MEG rsFC studies remain to be generalized to the case of scalp EEG, e.g., the functional connectome and its transient dynamics. The connectome (i.e., "all-to-all" brain rsFC) provides a global representation of brain rsFC encompassing all intra- and cross-RSN interactions (for review, see, e.g., Craddock et al., 2015; Friston, 2011), which allows, e.g., for a modelization of brain functional integration into graphs or a prior-free examination of disease-related disconnections. This whole-brain setup is also necessary for a consistent understanding of rsFC dynamics at short timescales (i.e., 1–10 s), where RSNs transiently split into sub-networks and establish cross-network coupling (for a review, see, e.g., de Pasquale et al., 2018), thus forming dynamic states of rsFC (for reviews, see Hutchison et al., 2013; O'Neill et al., 2018). Dynamic rsFC appears crucial for human brain functional integration (de Pasquale et al., 2016, 2012) and may be more sensitive than static rsFC to some physiological processes (Brookes et al., 2018) and pathological disconnections (Damaraju et al., 2014).

Here, we used simultaneous 306-channel MEG and 256-channel scalp EEG recordings at rest and compared directly the resulting electrophysiological connectomes, including their dynamic aspects. Under the hypothesis formulated by Siems et al. (2016) that rsFC is generated by cortical areas sufficiently large to cover both gyri and sulci and thus be detectable by both MEG and scalp EEG (for a detailed review on MEG and scalp EEG, see Harri and Puce, 2017), we expected the two modalities to yield similar static and dynamic rsFC patterns. Further, given the reported importance of gray/white matter separation for EEG source reconstruction (Gençer and Acar, 2004), we considered two versions of the EEG connectome: one based on a three-layer head model that does not discriminate gray/white tissue conductivity and the other, based on a five-compartment model that assigns different conductivity values. Extrapolating from Liu et al. (2018), we expected moderate MEG-EEG rsFC consistency when using the former, and good consistency when using the latter.

2. Materials and methods

2.1. Participants

Twenty-four healthy adult subjects (10 females; mean age ± SD: 26.0 ± 4.3 years; range: 20–35 years) took part in this study. All subjects were right handed according to the Edinburgh handedness inventory (Oldfield, 1971), had no prior history of neurological or psychiatric disorder and did not take any psychotropic drug. Each participant signed a written informed consent before scanning. The CUB – Hôpital Erasme Ethics Committee approved this study prior to participants' inclusion.

2.2. Data acquisition

Subjects underwent a resting-state session (eyes opened, staring at a fixation cross, 5 min) with simultaneous MEG and high-density EEG signal acquisition. Neuromagnetic activity was recorded (band-pass: 0.1–330 Hz, sampling frequency: 1 kHz) with a 306-channel whole-scalp MEG system installed in a light-weight magnetically shielded room (Maxshield™, Elekta Oy, Helsinki, Finland; now MEGIN, Cronton Healthcare), the characteristics of which have been detailed elsewhere (De Tiège et al., 2008). Fourteen subjects were scanned with a Neuromag Vectorview™ MEG (Elekta Oy, Helsinki, Finland) and the ten last subjects with a Neuromag Triux™ MEG (MEGIN, Cronton Healthcare, Helsinki, Finland) due to a system upgrade. The two neuromagnetometers have identical sensor layout (i.e., 102 magnetometers and 102 pairs of orthogonal planar gradiometers) but differ in sensor dynamic range. Of note, previous works mixing recordings from these two systems did not reveal significant changes in data quality (Marty et al., 2019; Naeije et al., 2019). Four coils tracked subjects' head position inside the MEG helmet. Neuroelectric activity was measured with a MEG-compatible, 256-channel scalp EEG system (low-pass: 450 Hz; sampling frequency: 1 kHz) based on low profile, silver chloride-plated carbon-fiber electrode pellets (MicroCel Geodesic Sensor Net with Net Amp GES 400, Electrical Geodesics Inc., Philips, Eugene, Oregon, USA). Its 257 passive electrodes were specifically designed to avoid EEG-induced magnetic artifacts. Further, electrodes were only 2-mm thick so they minimally hampered head positioning in the MEG helmet. The reference electrode was placed at Cz and all impedances were kept below 50 kΩ thanks to a conductive gel between each electrode and the skin. The location of the head position coils, scalp EEG electrodes, and approximately 200 scalp points were determined with respect to anatomical fiducials using an electromagnetic tracker (Fastrack, Polhemus, Colchester, Vermont, USA). Participant's high-resolution 3D T1-weighted cerebral magnetic resonance images (MRIs) were acquired on a 1.5 T MRI scanner (Intera, Philips, The Netherlands).

2.3. Data preprocessing

Signal space separation (Taulu et al., 2005) was applied offline to MEG data to subtract environmental magnetic noise and correct for head movements (Maxfilter™ v2.2, Elekta Oy, Helsinki, Finland). Bad EEG channels were detected and reconstructed with an automated pipeline adapted from Bigdely-Shamlo et al. (2015). Specifically, we selected three criteria to identify noisy electrodes: (i) too small windowed correlation (1 s window, threshold: 0.4 for at least two windows) of low-passed signals (40 Hz) with the other channels, contradicting the expected volume conduction, (ii) too large high-to-low frequency amplitude ratio (1–40 Hz vs 40–60 Hz, threshold: 5 SD above mean) characteristic of high-frequency noise, and (iii) too large wide-band amplitude (1–300 Hz, threshold: 5 SD above mean) detecting extreme signal deviations due to, e.g., momentary electrode-skin contact loss. Channels marked as bad were reconstructed using spherical spline interpolation from the other electrodes (Perrin et al., 1989). This pipeline was repeated until no more bad channels were detected, and at most three times. Note that bad channel detection was not necessary for MEG data.

Ocular, cardiac, and remaining system artifacts were further eliminated using an independent component analysis of the band-passed (1–40 Hz) MEG and EEG data separately (FastICA with dimension reduction to 30 components, hyperbolic tangent nonlinearity contrast) (Vigário et al., 2000). Artefactual components were identified by visual inspection and regressed out of the full-rank data (number of components removed for MEG: 3.0 ± 0.7, range: 2–5; for EEG: 6.6 ± 1.7, range: 3–11). The EEG data were then re-referenced to their average across all electrodes. For comparability of rsFC time series (see below), we ensured the synchronization of MEG and EEG signals by temporal re-alignment to a common trigger.

2.4. Forward modeling

Forward models were computed on the basis of the participants' MRI, which was segmented beforehand using the FreeSurfer software

(Martinos Center for Biomedical Imaging, Massachussetts, USA). The coordinate systems of MEG and EEG were co-registered to that of the MRI using the three anatomical fiducials for initial estimation and the head-surface points to manually refine the surface co-registration (Mrilab, Elekta Oy, Helsinki, Finland). Afterwards, a volumetric, regular 5-mm source grid was built using the Montreal Neurological Institute (MNI) template MRI and non-linearly deformed onto each participant's MRI with the software (SPM12, Wellcome Trust Centre for Neuroimaging, London, UK). Three orthogonal current dipoles were then placed at each grid point. Given the relative robustness of neuromagnetic signals to head conductivity inaccuracies (Gençer and Acar, 2004), we performed MEG forward modeling on this source space using the one-layer boundary element method (BEM) implemented in the MNE-C suite (Martinos Centre for Biomedical Imaging, Massachussets, USA). On the other hand, we considered two different forward models for scalp EEG: (1) a three-layer BEM (BEM_3) computed with the MNE-C suite and its default conductivity values $\sigma_{brain} = 0.3/\Omega m$, $\sigma_{skull} = 0.006/\Omega m$, and $\sigma_{scalp} = 0.3/\Omega m$, and (2) a five-compartment finite element model (FEM_5) computed with the integrated FieldTrip-Simbio toolbox (Vorwerk et al., 2018) and its default conductivity values $\sigma_{white\ matter} = 0.14/\Omega m$, $\sigma_{gray\ matter} = 0.33/\Omega m$, $\sigma_{cerebrospinal\ fluid} = 1.79/\Omega m$, $\sigma_{skull} = 0.01/\Omega m$, and $\sigma_{scalp} = 0.43/\Omega m$. The EEG forward models were re-referenced to their average across electrodes.

2.5. Source reconstruction

Cleaned MEG and EEG data were filtered in the alpha (α: 8–13 Hz) and the beta (β: 12–30 Hz) frequency bands. Minimum norm estimation (MNE; Dale and Sereno, 1993) was applied to reconstruct the sources of band-limited activity. The MEG noise covariance matrix was estimated individually for each subject from 5 min of empty-room data filtered in the relevant frequency band. The EEG noise covariance matrix was taken as the identity projected in the sensor subspace corresponding to the average reference. The regularization parameter was estimated in each case using the consistency condition derived in Wens et al. (2015). Three-dimensional dipole time series were projected on their direction of maximum variance, and their analytic source signal was reconstructed using the Hilbert transform.

We did not explicitly correct for the depth bias in these source data since functional connectivity measures (such as the envelope correlation described below) are scale invariant and thus unaffected by this bias. In fact, in this context, our source projection pipeline is rigorously equivalent to noise-normalized versions of MNE such as standardized low-resolution tomography (Pascual-Marqui, 2002).

2.6. Functional connectivity estimation

We quantified here intrinsic rsFC between two source time courses as their envelope correlation preceded by signal orthogonalization to correct for spatial leakage (Brookes et al., 2012). For static rsFC, envelopes were low-pass filtered below 1 Hz and temporal correlation was computed over the whole recording length (see Wens et al., 2014b, 2015). Dynamic rsFC estimation was similar, except that the low-pass was set to 10 Hz and correlations were computed over sliding windows (length: 10 s, step: 5 s; see de Pasquale et al., 2010; Wens et al., 2019), resulting in one rsFC estimate per time window.

Although our main focus was on the connectome, following Siems et al. (2016), we started by a quality control analysis of the seed-based static rsFC maps associated with five well-known MEG RSNs in their preferential frequency band (Wens et al., 2014a): the primary sensorimotor (SM1; seed MNI coordinates: [42,–26,54] mm; β band), auditory (A1; [54,–22,10] mm; β), and visual (V1; [20,–86,18] mm; α) networks as well as the default-mode (DMN; [–2,51,2] mm; α) and the fronto-parietal (FP; [34,20,44] mm; β) networks.

In the connectome approach, we estimated rsFC between signals summarizing the source-reconstructed activity within brain parcels. The brain was parcellated into 82 cortical areas using the automated anatomical labeling atlas (Tzourio-Mazoyer et al., 2002), from which we discarded deep brain structures such as the putamen, the pallidum, and the caudate area. We extracted the summary signal of each parcel as the principal component of all point source estimates falling within that parcel. The matrix gathering all rsFC estimates was symmetrized by averaging it with its transpose (as in Hipp et al., 2012), because asymmetries can be introduced by pairwise orthogonalization of the parcel signals. These asymmetries are indicative of leakage correction errors and may affect rsFC estimation quality (Palva et al., 2018). In principle, a better solution is to resort to the symmetric multivariate orthogonalization of Colclough et al. (2015). However, in our case, this algorithm would be ill-conditioned and thus not applicable, because the number of signals to orthogonalize (i.e., 82 in this parcellation) is larger than the number N_{sdof} of spatial degrees of freedom in our source-projected data. This number can be estimated as the rank of the forward model (Wens et al., 2015) and is reported in Table 1 (top row).

For the statistical comparisons described below, all resulting rsFC matrices (i.e., for each subject, and also for each time window in the dynamic case) were normalized by their whole-brain average in order to suppress global differences in rsFC levels between subjects and between MEG and scalp EEG. This procedure enabled us to focus on relative/regional rsFC (Kiebel and Holmes, 2007).

2.7. State classification of dynamic connectomes

To extract dynamic rsFC states from the sliding-window rsFC matrices, we applied a *k*-means clustering approach adapted from Allen et al. (2014) and O'Neill et al. (2015b). Briefly, group *k*-means clustering was performed by temporally concatenating the regional rsFC time series across subjects and using Lloyd's algorithm (Lloyd, 1982) with Pearson correlation of matrices as clusterization index. The initial clusters were set to the *k* first principal components of the data. To identify a reasonably small number of states needed to model the rsFC data, we applied this clustering for all parameters *k* between 1 and 50 and used the elbow criterion on the ratio of the within-cluster sum of squares to the between-cluster sum of squares. The optimal number of states was chosen as the abscissa of the point on the elbow curve that is farthest away from the chord joining the first ($k = 1$) and the last ($k = 50$) points. The resulting clusters at this optimal value were then interpreted as rsFC states. Each was characterized temporally by a binary time series identifying the windows where the state is active (by design, one and only one state was active in each window) and spatially by the average rsFC matrix across those windows.

2.8. Spatial similarity of connectivity patterns

Pearson correlation of group-level static rsFC maps or matrices was used to quantify the topographical similarity of RSNs or connectomes between the different modalities (i.e., MEG vs. EEG-BEM_3, MEG vs. EEG-FEM_5, and EEG-BEM_3 vs. EEG-FEM_5). Significance was assessed using one-tailed parametric tests at $p < 0.05$ against the null hypothesis that Fisher-transformed correlations follow a Gaussian with mean zero and SD $\frac{1}{\sqrt{N_{sdof}-3}}$. For the seed-based maps, N_{sdof} represents the number of spatial degrees of freedom, which was estimated as the rank of the forward model (Table 1, top row). For the connectome, we used $N_{sdof} = \frac{\rho(\rho-1)}{2}$ where ρ denotes the rank of the forward model restricted to the 82 parcel signals (Coquelet et al., 2017), see Table 1 (bottom row). Because the

Table 1
Number of spatial degrees of freedom in the three modalities.

N_{sdof}	MEG	EEG-BEM_3	EEG-FEM_5
Seed-based mapping	55	32	29
Connectome	360	148	100

higher spatial smoothness of EEG forward models led to smaller ranks than for MEG forward models (see Table 1), we applied these tests using the smallest value among the two N_{sdof}'s considered, leading to conservative correlation tests.

To quantify a possible effect of the EEG forward model type (BEM_3 and FEM_5) on MEG vs. EEG rsFC similarity, we performed two-tailed parametric tests of correlation differences. The null distribution was here a zero-mean Gaussian with SD $\frac{1}{\sqrt{M_{sdof}-6}}$ where M_{sdof} denotes the sum of the corresponding two values of N_{sdof}'s.

2.9. Spatial dissimilarity of connectivity matrices

To locate more precisely regional differences between connectomes, we considered the contrast between pairs of group-level static regional rsFC matrices. We applied two-tailed tests based on a null rsFC contrast distribution generated non-parametrically using 10^6 sets of random permutations of the modality label (MEG, EEG-BEM_3, EEG-FEM_5) before group averaging (Nichols and Holmes, 2002). The family-wise error rate associated with the multiple matrix entries to test was controlled by Bonferroni correcting the significance level $p < 0.05$ with the highest value among the two N_{sdof}'s considered (Table 1, second row), leading to somewhat conservative testing. The significant connections were mapped on the MNI glass brain using the BrainNet viewer (Xia et al., 2013), with the location of each extended parcel represented by its center.

2.10. Pairing of dynamic connectivity states

To compare the rsFC state dynamics across the different modalities, we sought to pair states using non-parametric (Spearman) correlation of their binary time series. Temporal pairing was detected statistically by one-tailed parametric tests against the null hypothesis that Fisher-transformed Spearman correlations follow a Gaussian with mean zero and SD $\sqrt{\frac{1.06}{N_{tdof}-3}}$. The number N_{tdof} of temporal degrees of freedom was here half the total number of sliding windows (to take their overlap into account) across all subjects. This estimate neglects possible long-time autocorrelations in rsFC time series as well as the contribution of epoch overlapping. The former increases noise on correlation estimates while the later decreases the noise. The significance level was set to $p <$ 0.05 Bonferroni corrected for the number of possible state pairs (i.e., $k_{modality\ 1} \times k_{modality\ 2}$). The cross-modality spatial similarity of significant rsFC state pairs was then examined using the Pearson matrix correlations described above.

2.11. Temporal similarity of envelope signals

To further illustrate the possible commonalities or discrepancies identified in rsFC estimation based on slow envelope correlation, we directly compared MEG and EEG envelope signals via their temporal Pearson correlation, for each brain parcel, EEG forward model, and frequency band. This MEG-EEG envelope similarity was derived separately for the two envelope filtering schemes (1-Hz low pass as used for static rsFC and 10-Hz as used for dynamic rsFC). The Fisher transform of these correlation values were then averaged within five distinct areas (frontal, parietal, occipital, cingulate, and temporal) and subjected to paired, two-tailed t tests to investigate possible effects of location (i.e., 5 areas; 10 tests per envelope filter totaling to 20) or envelope filter (i.e., 1-Hz vs. 10-Hz low pass; 1 test per region totaling to 5). The significance level was set to $p < 0.05$ Bonferroni corrected for the total number of tests (i.e., 25 x 2 EEG forward models x 2 frequency bands). Of note, we did not use an ANOVA here because the two factors of interest are *a priori* interdependent. Indeed, envelope signals are correlated across brain regions due to the existence of rsFC, and by construction their 1-Hz low-pass component is part of their 10-Hz low-pass component. It is also noteworthy that these statistics built from a set of individual correlation coefficients combine both the estimation errors due to finite time sampling (whose variance is affected by the low-pass filters since they lead to different amounts of temporal degrees of freedom) and other sources (e.g., biological) of inter-subject variability. In our data, the latter turned out to dominate the finite-sampling errors.

2.12. Data and code availability statement

MEG and EEG data used in this study will be made available upon reasonable request to the corresponding author.

3. Results

3.1. Network maps

Fig. 1 depicts the seed-based static rsFC maps of five RSNs obtained using MEG, EEG-BEM_3, and EEG-FEM_5. All classical primary RSNs, i.e., SM1, A1, and V1 were recognizable within each modality, and the corresponding cross-modality similarities were all significant (Pearson correlation $R \geq .54$, $p < 10^{-3}$ in all cases). Usage of FEM_5 instead of BEM_3 increased the similarity between MEG and EEG for the A1 RSN (correlation difference $|\Delta R| = .27$, $p = 10^{-4}$) but not for the SM1 or the V1 RSNs ($|\Delta R| \leq .05, p \geq .7$). The typical antero-posterior interactions of the DMN were observable with MEG and EEG-FEM_5, whose maps were similar ($R = .75$, $p = 3 \times 10^{-7}$), but absent with EEG-BEM_3 where frontal rsFC dominated, leading to maps dissimilarity ($R \leq -.18, p \geq .8$) and a strongly significant increase of MEG-EEG similarity when using FEM_5 instead of BEM_3 ($|\Delta R| = .94$, $p = 2 \times 10^{-17}$). Finally, the topography of the MEG FP map disclosed a notable dissimilarity with those of EEG-BEM_3 and EEG-FEM_5 ($R \leq .3$, $p \geq .06$), the two latter being similar ($R = .92$, $p = 3 \times 10^{-16}$), with no effect of forward model type ($|\Delta R| = .05$, $p = .3$). The MEG FP map appeared mostly sensitive to the intra-hemispheric fronto-parietal connection, while those of EEG rather disclosed the inter-hemispheric frontal connection.

3.2. Static connectomes

Fig. 2 illustrates the static rsFC matrices obtained with each modality in both α and β frequency bands. Qualitatively, the MEG connectomes displayed relatively focal rsFC patterns peaking mainly in the parietal, occipital, and cingulate areas (Fig. 2, leftmost column). Of note, MEG rsFC was estimated by pooling data from two distinct systems (Vectorview vs. Triux), but they did not exhibit a significant dependence in the system type. Indeed, a regression analysis of individual MEG rsFC with a categorical regressor identifying the corresponding system type did not reveal any significant correlation (Pearson correlation test at $p < 0.05$ Bonferroni corrected for the effective number of independent connections, see the second row of Table 1). Similar parieto-occipito-cingular rsFC patterns were observable with EEG, but EEG also disclosed substantial β-band frontal rsFC (Fig. 2, center columns). Notably, EEG rsFC appeared blurrier than MEG rsFC (in line with the higher smoothness of EEG as assessed in Table 1). There was also no clear effect of forward modeling type (BEM_3 and FEM_5) on the EEG connectomes.

The correlation analysis of these rsFC matrices demonstrated statistically that each modality yielded significantly similar connectomes in both α and β frequency bands ($R \geq .23$, $p \leq .01$), with no significant effect of EEG forward modeling type on MEG-EEG similarity ($|\Delta R| \leq .05$, $p \geq .79$). Incidentally, this last result also suggests that changing the precise conductivity values (which were quite different, e.g., BEM_3 skull conductivity was 60% the value for FEM_5) does not substantially impact EEG rsFC estimation. As a control, we re-derived the EEG-BEM_3 connectome using the FEM_5 skull conductivity value and obtained virtually identical rsFC matrices (matrix correlation $R \geq .99$).

To examine possible topographical differences between EEG and MEG connectomes, we further considered the contrast of regional rsFC values,

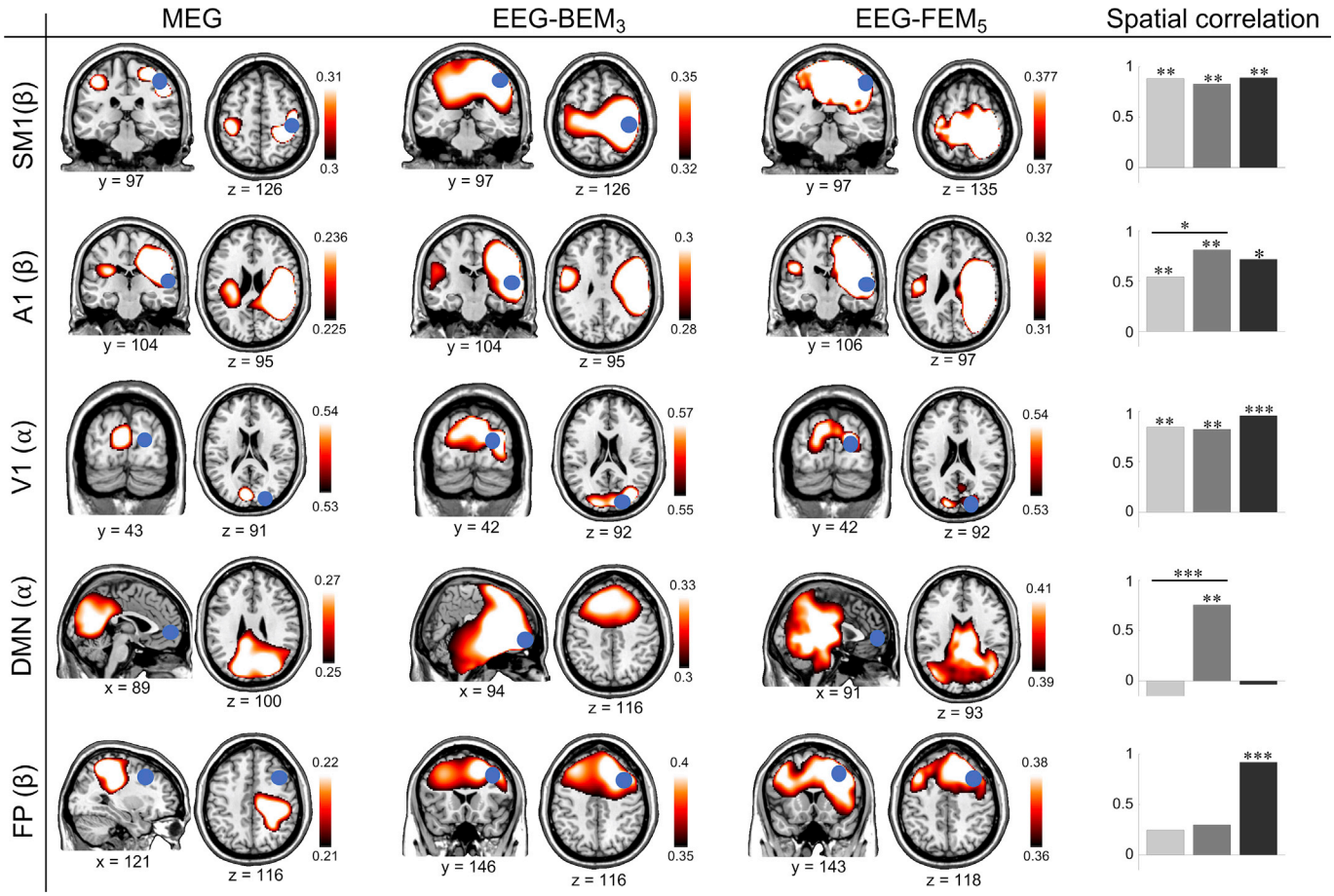

Fig. 1. Seed-based static rsFC mapping of selected RSNs superimposed on the MNI brain with MEG (**first column**), EEG-BEM$_3$ (**second column**), and EEG-FEM$_5$ (**third column**). Seeds are represented by blue dots. The location of coronal and axial MRI slices is indicated by MNI x, y, or z coordinates below each slice. Thresholds of RSN maps were set for visualization purposes. The cross-modality spatial similarity (light gray: MEG vs EEG-BEM$_3$, dark gray: MEG vs EEG-FEM$_5$, black: EEG-BEM$_3$ vs EEG-FEM$_5$), as well as the changes in MEG-EEG similarity due to EEG forward modeling, are also shown (**fourth column**; *: $p < 10^{-3}$, **: $p < 10^{-6}$, ***: $p < 10^{-15}$).

i.e., standardized to the whole-brain average rsFC (which was systematically higher with EEG than MEG, see Fig. 2). In both α and β frequency bands and independently of the EEG forward model type, EEG showed higher regional rsFC within nodes of the frontal region, and MEG higher regional rsFC within the parieto-occipital region (Fig. 3 left and middle, second and third rows). We further observed higher regional α-band rsFC between the frontal and the parietal regions with MEG compared to EEG-BEM$_3$ (Fig. 3 left, second row) but not compared to EEG-FEM$_5$ (Fig. 3 middle, second row). This effect of EEG forward modeling could also be seen on the direct comparison of the two EEG modalities, mainly in the α band (Fig. 3 right, second row) and scarcely in the β band (Fig. 3 right, third row).

Findings of increased frontal and decreased parieto-occipital regional rsFC for EEG compared to MEG were considered to be potentially driven by inhomogeneous topography of brain-sensor distances associated with MEG recordings done in the sitting position (i.e., posterior sources might have been closer to MEG sensors than frontal sources as the head typically lays at the back of the MEG helmet for obvious comfort reasons). We therefore compared the group-averaged brain-sensor distances (specifically, the distance between each brain parcel and the closest sensor) obtained for the MEG helmet and the scalp EEG sensor net (Fig. 4). The MEG sensors were 2–4 cm farther away than the scalp EEG electrodes depending on the parcel, with minimal differences in the parieto-occipital region where MEG regional rsFC dominated, and maximal differences in the frontal region where scalp EEG regional rsFC dominated. We thus hypothesized a relationship between regional rsFC contrasts and the MEG vs. EEG differences in brain-sensor distances. To confirm this qualitative observation, we repeated the contrast analysis after regressing out from each matrix entry the distance differences for the two corresponding brain parcels. The rsFC contrasts and their double regression models are shown in Fig. 5 and no significant residual MEG vs. EEG contrast subsisted.

3.3. Connectivity state dynamics

The cross-modality similarity of dynamic rsFC states was then investigated. The optimal number of states was quite similar across modalities and frequency bands, i.e., 7–10 (Table 2). State-specific rsFC patterns are detailed in Figs. 6 and 7.

Temporal correlations of state time series revealed poor correspondence between MEG and EEG. In the α band, we identified only one significant pair of corresponding MEG and EEG states when using BEM$_3$, two when using FEM$_5$ (Spearman correlation, $R \geq .13$, $p \leq 5 \times 10^{-4}$). We obtained no temporal pairing in the β band ($R \leq .09$, $p \geq .01$). As can be viewed from Fig. 6, the three significant state pairs were also spatially similar (Pearson correlation, $R \geq .55$, $p \leq 7 \times 10^{-10}$). The MEG-EEG pair identified when using BEM$_3$ involved primarily rsFC between left temporal and bilateral frontal regions (Fig. 6, green arrow). Those obtained with FEM$_5$ corresponded to occipital (Fig. 6, top orange arrow) and bilateral sensorimotor rsFC (Fig. 6, bottom orange arrow). This somehow restricted correspondence between MEG and EEG states contrasted with the comparison of the two EEG modalities, which revealed significant

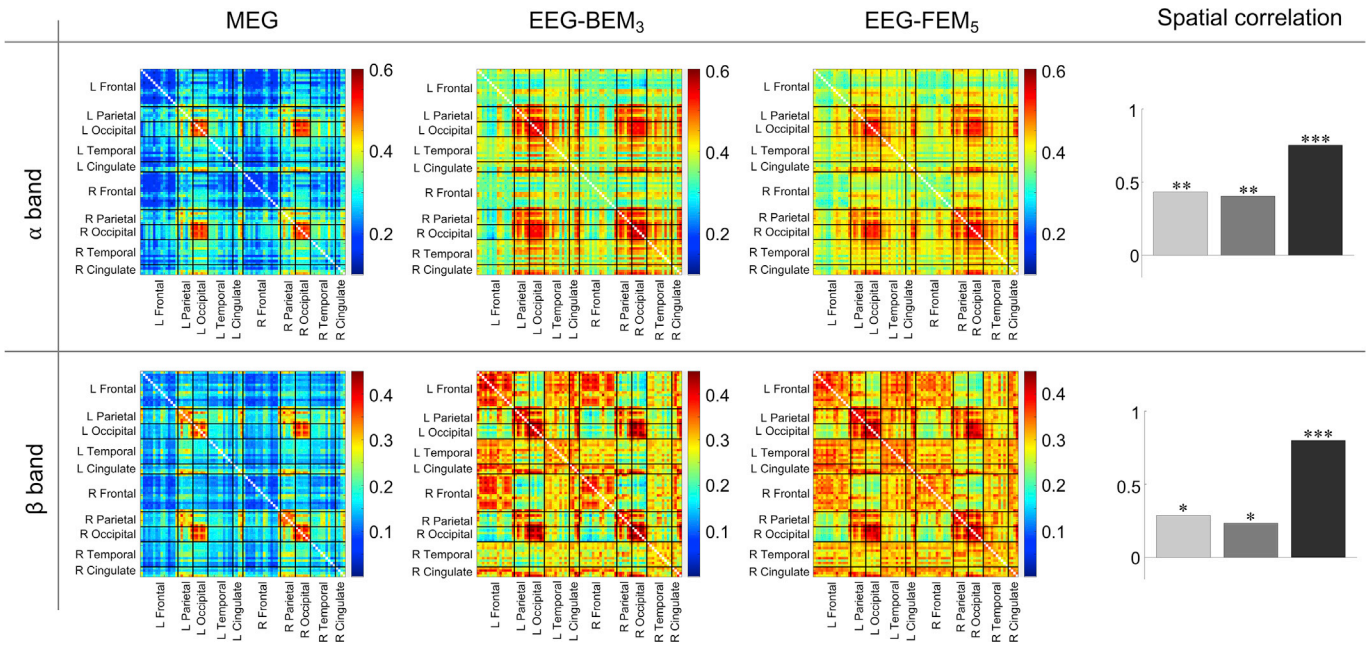

Fig. 2. Static functional connectomes with MEG (**first column**), EEG-BEM$_3$ (**second column**), and EEG-FEM$_5$ (**third column**) in the α (**top**) and β (**bottom**) frequency bands. Brain parcels are gathered by hemisphere (L: left, R: right) and lobe (frontal, parietal, occipital, temporal, and cingulate). Thresholds of rsFC matrices were set consistently across the three modalities. The cross-modality spatial similarity (light gray: MEG vs EEG-BEM$_3$, dark gray: MEG vs EEG-FEM$_5$, black: EEG-BEM$_3$ vs EEG-FEM$_5$) is also displayed (**fourth column**; *: $p < 0.05$, **: $p < 10^{-4}$, ***: $p < 10^{-15}$).

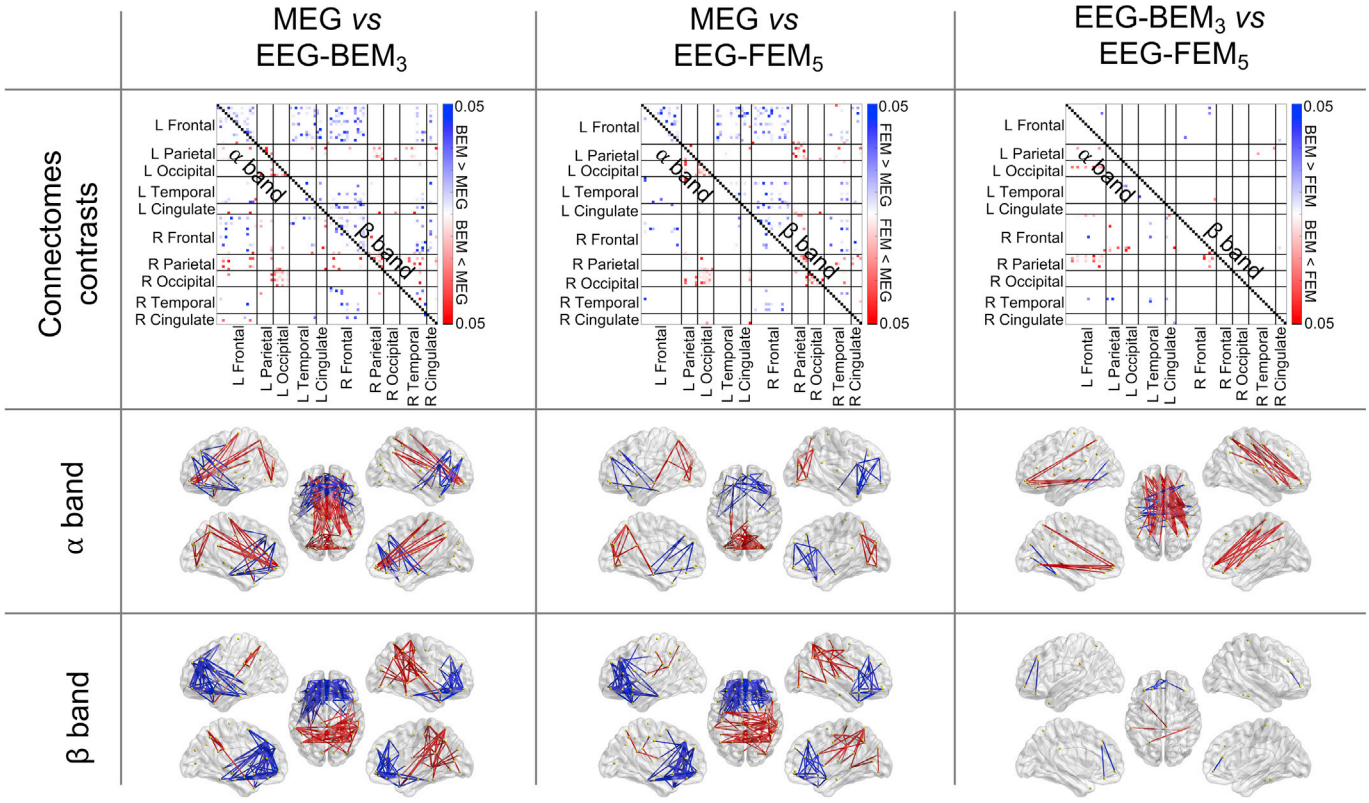

Fig. 3. Cross-modality contrasts of static regional connectome rsFC matrices comparing MEG vs. EEG-BEM$_3$ (**left**), MEG vs. EEG-FEM$_5$ (**middle**), and EEG-BEM$_3$ vs. EEG-FEM$_5$ (**right**). Significant corrected p values are shown as matrices (**first row**) wherein the parcels are gathered by hemisphere (L: left, R: right) and lobe (frontal, parietal, occipital, temporal, and cingulate). The lower and upper triangles of each matrix correspond respectively to α and β frequency bands. Connections with significant contrast are also shown on the MNI glass brain (α: **second row**; β: **third row**).

pairing for a majority of states. Most of EEG-BEM$_3$ states corresponded temporally to one or two EEG-FEM$_5$ states ($R \geq .14$, $p \leq 1.4 \times 10^{-4}$), with each pair consisting of spatially similar rsFC matrices ($R \geq .48$, $p \leq 1.4 \times 10^{-7}$). The situation in which a state is split into two might be explained by the differences in state numbers across the two EEG modalities. In the α band (Fig. 6), where we identified fewer states with EEG-

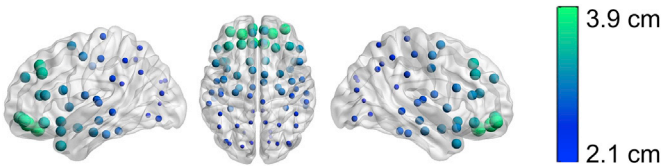

Fig. 4. Difference in brain-sensor distances from the center of each parcel to the MEG helmet vs. the scalp EEG net.

FEM_5 than with EEG-BEM_3, three EEG-BEM_3 states appeared mixed into two EEG-FEM_5 states. Conversely, in the β band (Fig. 7), there was more states with EEG-FEM_5 than with EEG-BEM_3 and two EEG-FEM_5 states appeared mixed into one EEG-BEM_3 state.

3.4. Envelope signals

Fig. 8 shows that the pattern of MEG-EEG dissimilarities observed in frontal static rsFC and in rsFC state dynamics could also be identified directly at the level of the envelope signals. In all cases, the MEG and EEG envelope time courses were significantly more correlated in the parieto-occipital region than in the frontal area ($p < 3.1 \times 10^{-4}$; Fig. 8, left). Cross-modal envelope similarity was also significantly higher with the 1-Hz low pass than with the 10-Hz low pass ($p < 6.9 \times 10^{-5}$; Fig. 8, left). This is reminiscent of the poor correspondence between MEG and EEG rFC states. Fig. 8 (right) presents excerpts of β-band envelope time courses at the right SM1 seed (see Fig. 1, top) and its left homologous source. Even on these short segments, this example illustrates the loss of correspondence between MEG and EEG signals when turning from slow to fast envelope.

4. Discussion

In the present study, we directly compared well-known RSNs as well as the whole-brain rsFC connectome together with its state dynamics, obtained from simultaneously-recorded MEG and scalp high-density EEG resting-state data. Besides evidencing fairly similar RSN patterns, we found that intrinsic functional connectivity patterns reconstructed from MEG and scalp EEG resting-state data differ in their sensitivity to frontal and parieto-occipital rsFC. This difference mainly impacts the FP RSN and seems to relate to that anterior MEG sensors are typically more distant from the brain than posterior sensors. Distinguishing between gray and white matter affects the estimation with scalp EEG of antero-posterior rsFC and appears necessary to recover the DMN as observed with MEG. Finally and importantly, we found little agreement between modalities in state temporal dynamics, which appeared rooted in the dissimilarity of fast envelope fluctuations (i.e., above 1 Hz). This suggests that MEG and EEG are sensitive to different components of transient neural functional integration.

4.1. Similar static rsFC patterns between MEG and scalp EEG

The observation that both MEG and scalp EEG led to similar RSN patterns (except for the FP RSN) is in line with previous works (Liu et al., 2018, 2017; Siems et al., 2016). Worth mentioning, subjects kept they eyes closed in Siems et al. (2016) and open in the present study. The convergence of our findings shows that MEG and EEG concur for RSN mapping regardless of this experimental difference. Our study generalizes this cross-modal agreement to the whole-brain connectome. Still, we identified topographical differences, i.e., MEG regional rsFC was lower in the frontal areas and higher in the occipito-parietal areas compared with scalp EEG. Accordingly, the consistency of MEG and EEG envelope signals was least in the frontal area. These differences appeared imputable to inhomogeneities in the relative distance of the MEG vs. EEG sensors to brain sources. This can be explained by that increasing brain-sensor distance decreases the MEG/EEG signal amplitude (for a review, see, e.g., Harri and Puce, 2017), which in turn affects rsFC estimation. Compared to EEG electrodes, frontal MEG sensors were indeed further away from the scalp (about 4 cm) than posterior sensors (about 2 cm). Assuming comparable noise levels across MEG sensors, this signal loss induces lower signal-to-noise ratio and thus lower MEG

Table 2
Number of states for each modality and frequency band.

	MEG	EEG-BEM_3	EEG-FEM_5
α band	8	9	8
β band	7	8	10

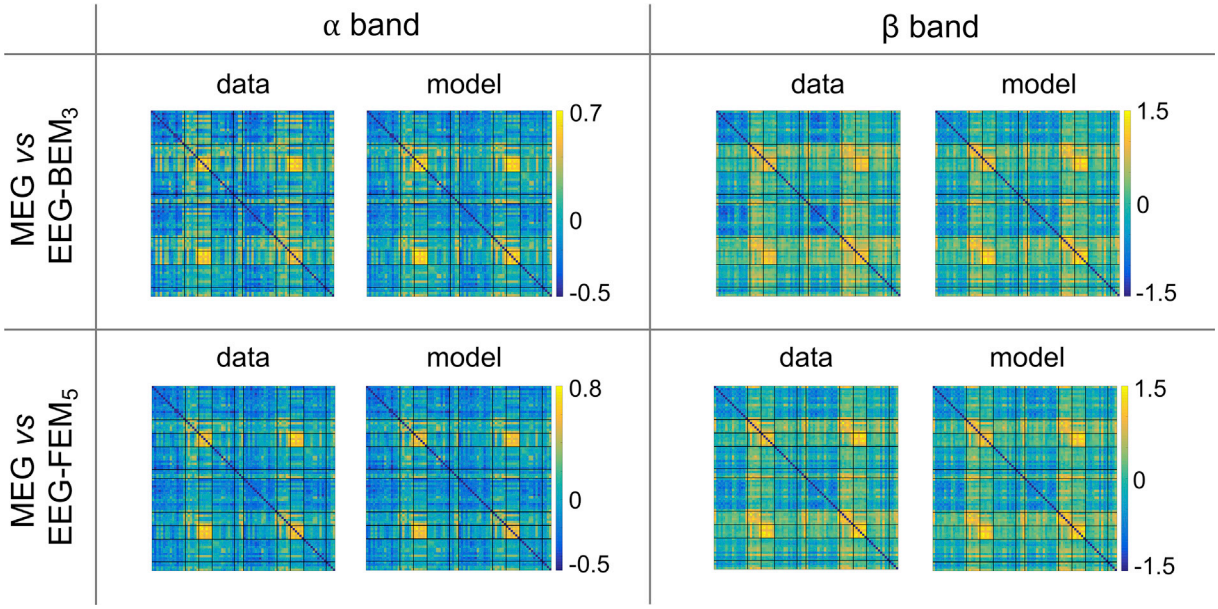

Fig. 5. Regression analysis of the effect of brain-sensor distance on regional rsFC contrasts. For each matrix entry, we modeled the contrast of rsFC between the two parcels using double regression by the two corresponding distance differences. The rsFC contrast matrices and their regression models are shown for the comparison of MEG vs. EEG-BEM_3 (**top**) and EEG-FEM_5 (**bottom**) in the α (**left**) and the β (**right**) bands.

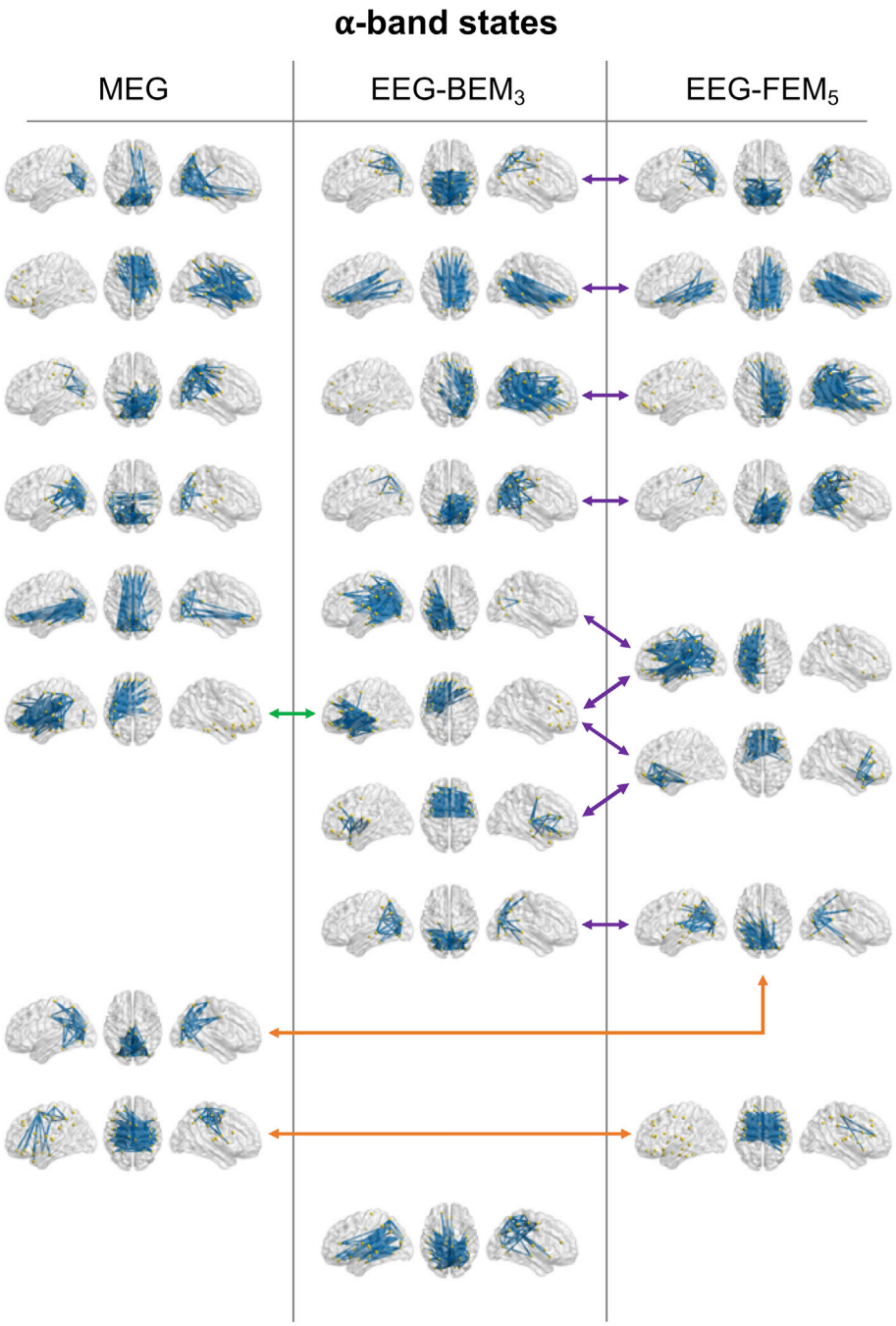

Fig. 6. States of dynamic rsFC in the α band identified with MEG (**left**), EEG-BEM_3 (**middle**), and EEG-FEM_5 (**right**). Their spatial signature is illustrated by showing the 5% strongest connections on the MNI glass brain. Temporal pairing between states is represented by arrows (green between MEG and EEG-BEM_3, orange between MEG and EEG-FEM_5, and purple between EEG-BEM_3 and EEG-FEM_5).

rsFC estimation within frontal nodes compared to within posterior nodes. This effect may explain why the FP RSN obtained with MEG did not reveal the inter-hemispheric frontal connection (to which EEG appeared sensitive) but only the intra-hemispheric fronto-parietal connection. Of note, this bias towards posterior rsFC could be less prominent in MEG systems based on different sensor layouts. For example, it has been suggested that CTF MEG may better identify frontal rsFC than the Neuromag system used here (Sjøgård et al., 2019). That said, the effect of doubling the brain-sensor distance will necessarily decrease signal amplitude by a factor between four (for magnetometers) and eight (for gradiometers), so we expect this problem to remain whatever the cryogenic MEG system used. In the future, the issue of brain-sensor distance should be completely solved by the rise of wearable scalp neuromagnetometers (Boto et al., 2018). Further, scalp MEG based on optically pumped magnetometers (OPMs) should bring substantial increase in signal-to-noise ratio and spatial focality compared with current MEG systems based on superconducting quantum interference devices (SQUIDs). Accordingly, we envision that OPMs will eventually provide higher spatial resolution imaging of rsFC than SQUIDs or EEG, at least once multi-channel systems with sufficiently many OPMs (i.e., more than the number of spatial degrees of freedom in MEG, see first row of Table 1) will become available. As

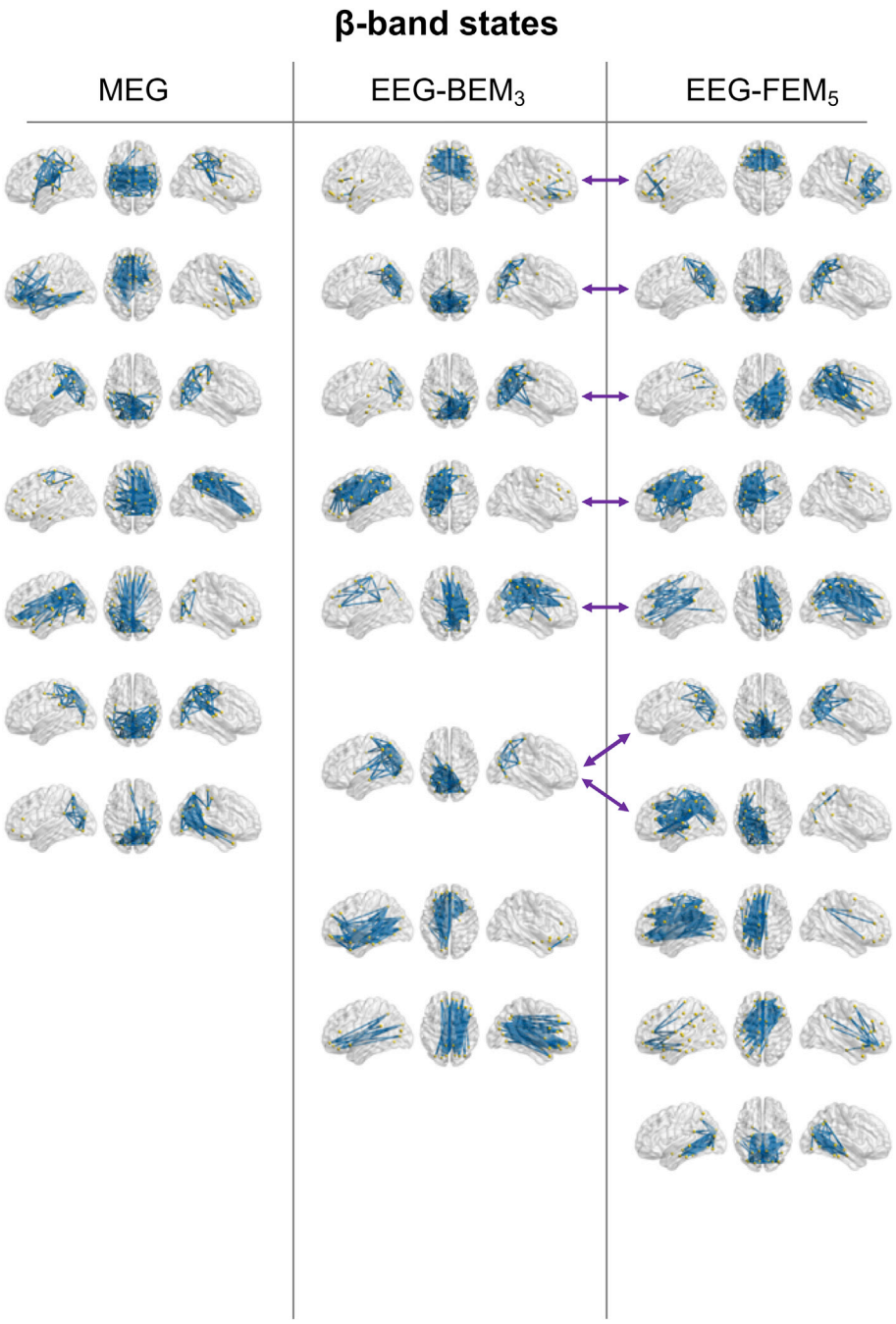

Fig. 7. States of dynamic rsFC in the β band identified with MEG (**left**), EEG-BEM_3 (**middle**), and EEG-FEM_5 (**right**). Their spatial signature is illustrated by showing the 5% strongest connections on the MNI glass brain. Temporal pairing between states is represented by arrows (purple between EEG-BEM_3 and EEG-FEM_5).

such, this novel technology might ultimately become the reference technique for electrophysiological rsFC investigations, overpassing the performances of scalp EEG and cryogenic MEG.

In any case, we conclude that SQUID-based MEG and scalp EEG both allow to map similar static rsFC patterns. Notwithstanding the brain-sensor distance bias, this convergence is in line with the hypothesis of Siems et al. (2016) that static rsFC and RSNs are generated by cortical areas large enough to cover both sulci and gyri, thus mitigating the differences in EEG and MEG sensitivity to precise source orientation (for a review, see Harri and Puce, 2017) and to field distortion by skull conductivity or conductivity anisotropy (Gençer and Acar, 2004; Wolters et al., 2006), at least at the group level. However, this hypothesis is challenged by our analysis of dynamic connectomes.

4.2. Discordant state dynamics between MEG and EEG

The state models for MEG and EEG rsFC revealed a similar complexity (i.e., number of states). We therefore expected a high degree of concordance between MEG and EEG states. However, their temporal correspondence appeared marginal at best (especially compared to the substantial pairing observed between EEG-BEM_3 vs. EEG-FEM_5 states). This could be due to strong statistical errors in short-time correlation estimates (a general limitation of dynamic rsFC, see, e.g., Hutchison et al., 2013), which could be independent in the two modalities and thus hamper their comparability. Spatial leakage mis-correction associated with orthogonalization asymmetry could also contribute to this discrepancy. Still, their impact may be less drastic than expected at the

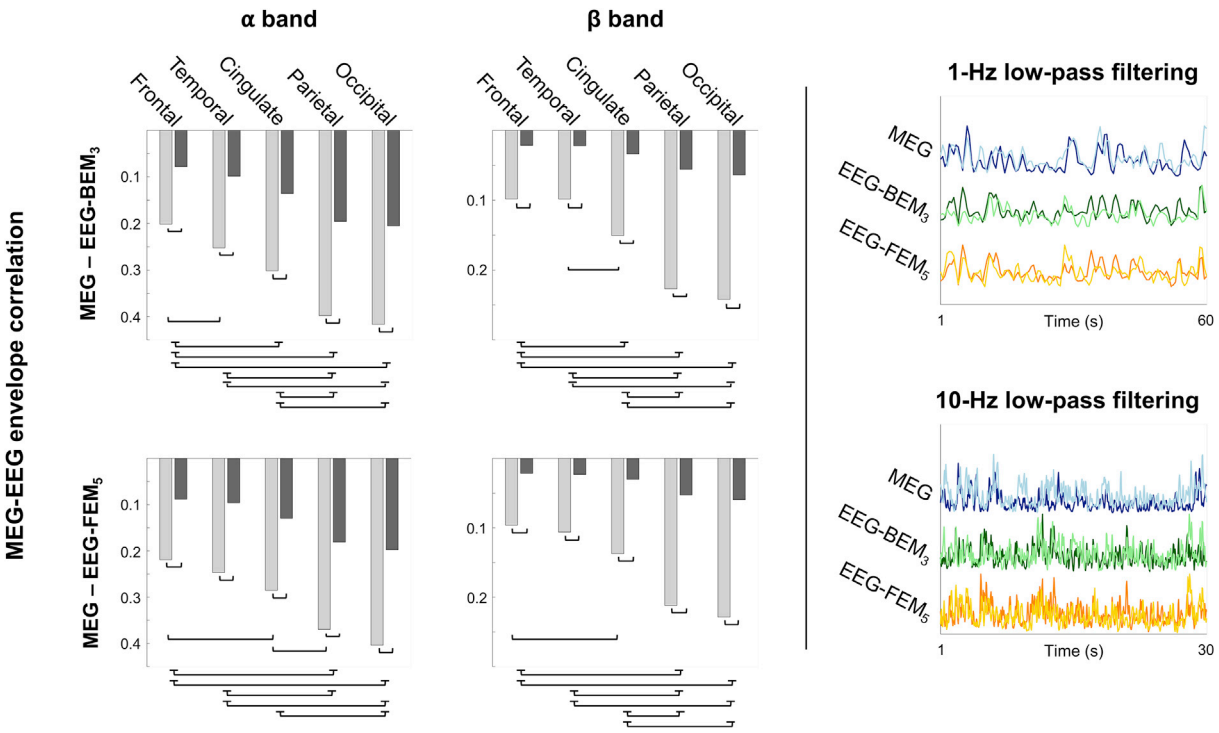

Fig. 8. Cross-modality similarity of source envelope signals. **Left:** The MEG vs. EEG temporal correlation of α- and β-band envelopes is shown for the two low-pass filters (light gray: 1 Hz, dark gray: 10 Hz) and the two EEG forward models. Correlations were averaged per brain regions (frontal, temporal, cingulate, parietal, and occipital). Significant effects according to *t* tests with Bonferroni correction are also emphasized. **Right:** Illustration of the effect of modality and low-pass filtering on the envelope similarity of the right SM1 seed (location indicated on Fig. 1, top) and its left-hemispheric homologous source.

level of rsFC states, given the averaging process included in *k*-means clustering (see also Wens et al., 2019, for a related discussion). Another, more basic factor independent of any rsFC estimation details is the observed lack of temporal correspondence between MEG and EEG high-frequency envelope signals used for dynamic rsFC estimation. This contrasted with the temporal similarity of their slow, 1-Hz low-pass filtered counterpart that underlies static rsFC. One possible explanation for this low/high envelope frequency dichotomy relies on the observation that static rsFC corresponds to an average of rsFC state patterns (weighted by their fractional occupancy). Temporal summation leads to spatial smoothing and thus lesser sensitivity to the precise location and orientation of rsFC neural generators. For the same reason, low-pass filtering of spatio-temporal data such as the source envelope signals effectively induces a spatial smoothing. The convergence of MEG and EEG static rsFC may thus be explained by this smoothing effect instead of the "extended-area" hypothesis (Siems et al., 2016). Furthermore, this smoothing effect breaks down at the shorter timescales of dynamic rsFC, which may have higher sensitivity to different neural generators of the spontaneous neuromagnetic and neuroelectric fields, leading to poor temporal correspondence in MEG and EEG signals and thus discrepancies in rsFC state allocation. In this context, MEG and scalp EEG appear complementary (rather than redundant) techniques to study the dynamic functional network organization of the human brain (de Pasquale et al., 2018). It will be interesting in future works to examine whether recent MEG discoveries about sub-second state dynamics (Baker et al., 2014) including transient phase couplings at rest (Vidaurre et al., 2018), dynamic core networks (de Pasquale et al., 2016, 2012), and cross-network synchrony and metastability (Wens et al., 2019) translate to scalp EEG.

Besides, this complementarity raises the interesting question of the advantages of a complete MEG-EEG integration for rsFC analysis. Combining MEG and EEG data for source estimation is thought to improve localization accuracy and lessen spatial extent (Liu et al., 2002), however the generalization to the study of the intrinsic functional connectome based on envelope rsFC remains to be developed. This represents a challenging but potentially rewarding methodological advance. More modestly, we limited the goal of our study to the comparison of MEG and EEG to probe intrinsic connectivity.

4.3. Electrophysiological static rsFC investigations can be performed with scalp EEG

This study demonstrates that static electrophysiological rsFC analyses and RSN mapping can be performed with scalp EEG, which concurs with previous studies (Siems et al., 2016; Liu et al., 2017, 2018) but extends these to the whole-brain functional connectome. Pragmatically, this observation enables moving the field of static rsFC from MEG, whose availability is limited by the high costs related to its cryogenics and heavy shielding (Baillet, 2017), to EEG, which is comparably cheaper (even in its high-density version) and more commonly accessible. In particular, it is also bound to broaden the clinical applications of electrophysiological rsFC investigations. Several RSNs have been identified, mainly with fMRI, as being involved in the pathophysiology of a wide spectrum of neurological or psychiatric disorders (Fox, 2018; Fox and Greicius, 2010). The ability to use scalp EEG rather than fMRI in clinical assessments of static rsFC appears critical since several brain disorders (e.g., stroke, Alzheimer's disease, epilepsy) are characterized by altered neurovascular coupling that impacts the fMRI signal (for a review, see, e.g. D'Esposito et al., 2003). Investigating the electrophysiological correlates of static rsFC with scalp EEG thus emerges as a potential breakthrough for clinical neurosciences.

In this context, the DMN appears as a relevant clinical target since it plays a key role in several brain disorders (Fox, 2018; Fox and Greicius, 2010), notwithstanding its centrality for physiological brain organization as well (see, e.g., de Pasquale et al., 2012; Wens et al., 2019). It is well established that electrophysiological mapping of the DMN is feasible with MEG (de Pasquale et al., 2010; Wens et al., 2014b). Importantly,

Sjøgård et al. (2019) demonstrated that imaging all the nodes of the DMN including the posterior medial cortices (which are critical to physiological and clinical conditions; for a review, see Leech and Sharp, 2014) requires source reconstruction based on MNE rather than Beamforming. This is why we relied on MNE in our rsFC analysis pipeline. This study confirms that full DMN mapping is possible with scalp EEG and MNE source projection, provided that head models are estimated with relatively precise methods distinguishing between gray and white matter (e.g., FEM_5). This observation argues for the use of advanced, state-of-the-art volume conduction models, such as the recent 12-compartment FEM developed by Liu et al. (2017). This being said, the impact of precise head modeling was moderate at best for the other RSNs for which a semi-realistic BEM_3 model appeared sufficient. The reason why only antero-posterior connections of the DMN required proper modelization of the gray/white matter separation remains unclear.

When envisioning clinical applications, two key factors must also be considered to properly assess rsFC: recording length and number of electrodes. Liuzzi et al. (2017) showed that robust estimation of individual rsFC with MEG would require at least 10 min-long resting-state sessions. Here our recordings lasted only 5 min, which is why we conducted group-level analyses only. Ultimately, however, EEG rsFC should be robustly estimated based on individual data to be clinically useful. Determining the minimal recording length necessary to obtain robust single-subject connectomes is thus an important factor to be considered in future works. Regarding the number of electrodes, clinical systems typically contain 32 or 64 electrodes. Here, we focused on 256-channel scalp EEG, but recordings across densely-packed electrodes are highly redundant due to field spread and volume conduction, both of which effectively act on the scalp potential topography as a spatial low-pass filter. Accordingly, we estimated that the 256 electrode signals entailed only about 30 degrees of freedom. This means that 32-channel scalp EEG may in theory be sufficient to capture rsFC, at least in the limit of large signal-to-noise ratio. More realistically though, to compensate for noise and bad channels it is reasonable to require at least twice as many electrodes. Thus, we recommend 64-channel scalp EEG as the minimal setup to study rsFC. This conclusion agrees with the systematic examination by Liu et al. (2018) of the sensor count effect on RSN maps.

4.4. Are MEG and scalp EEG complementary for electrophysiological dynamic rsFC investigations ?

Clinical value is less established for dynamic than for static rsFC, although promising results already emerged (Hutchison et al., 2013). Here, the divergence between MEG and scalp EEG rsFC dynamics suggests the added value of simultaneous MEG/EEG recordings. This combination and multimodal integration of electrophysiological techniques currently remains confined to research centers, where it could bring new insights into the dynamic integration structure of the human brain, as was discussed above. Still, together with the emergence of wearable scalp OPM-based MEG systems (Boto et al., 2018), the conjunction of simultaneous MEG/EEG with rsFC analysis may eventually revolutionize the position of functional mapping of brain networks in the clinics.

Author contribution section

N.C., X.D.T., and V.W. designed study; N.C., F.D., L.R., M.B., and V.W. acquired data; N.C. and V.W. contributed to analytical tools; N.C., X.D.T., and V.W. analysed data; N.C., X.D.T, F.D., L.R., M.B., S.G, P.P, and V.W wrote and reviewed the manuscript.

Acknowledgments

This study was supported by the Action de Recherche Concertée Consolidation (ARCC, “Characterizing the spatio-temporal dynamics and the electrophysiological bases of resting state networks”, ULB, Brussels, Belgium), the Fonds Erasme (Research Convention “Les Voies du Savoir”, Brussels, Belgium) and the Fonds de la Recherche Scientifique (Research Convention: T.0109.13, F.R.S. - FNRS, Brussels, Belgium). Nicolas Coquelet has been supported by the ARCC and is supported by the Fonds Erasme (Research Convention “Les Voies du Savoir”, Brussels, Belgium). Xavier De Tiège is Postdoctorate Clinical Master Specialist at the FRS-FNRS. Florian Destoky and Mathieu Bourguignon are supported by the program Attract of Innoviris (Research Grant 2015-BB2B-10, Brussels, Belgium). Mathieu Bourguignon is also supported by the Marie Sklodowska-Curie Action of the European Commission (Research Grant: 743562) and by the Spanish Ministery of Economy and Competitiveness (Research Grant: PSI2016-77175-P). Lillia Roshchupkina is F.R.S. - FNRS Research Fellow and was previously supported by a ULB Mini-ARC grant.

The MEG project at the CUB Hôpital Erasme is financially supported by the Fonds Erasme (Research Convention “Les Voies du Savoir”, Brussels, Belgium). The high-density EEG project at the CUB Hôpital Erasme has been financially supported by the CUB Hôpital Erasme (Medical Council Research Grant) and by the F.R.S. - FNRS.

The authors would like to thank Maribel Pulgarin Montoya for her help in part of the simultaneous MEG and high-density EEG recordings.

References

Allen, E.A., Damaraju, E., Plis, S.M., Erhardt, E.B., Eichele, T., Calhoun, V.D., 2014. Tracking whole-brain connectivity dynamics in the resting state. Cerebr. Cortex 24, 663–676. https://doi.org/10.1093/cercor/bhs352.

Baillet, S., 2017. Magnetoencephalography for brain electrophysiology and imaging. Nat. Neurosci. 20, 327–339. https://doi.org/10.1038/nn.4504.

Baker, A.P., Brookes, M.J., Rezek, I.A., Smith, S.M., Behrens, T., Probert Smith, P.J., Woolrich, M., 2014. Fast transient networks in spontaneous human brain activity. Elife 3, e01867. https://doi.org/10.7554/eLife.01867.

Bigdely-Shamlo, N., Mullen, T., Kothe, C., Su, K.-M., Robbins, K.A., 2015. The PREP pipeline: standardized preprocessing for large-scale EEG analysis. Front. Neuroinf. 9, 16. https://doi.org/10.3389/fninf.2015.00016.

Boto, E., Holmes, N., Leggett, J., Roberts, G., Shah, V., Meyer, S.S., Muñoz, L.D., Mullinger, K.J., Tierney, T.M., Bestmann, S., Barnes, G.R., Bowtell, R., Brookes, M.J., 2018. Moving magnetoencephalography towards real-world applications with a wearable system. Nature 555, 657–661. https://doi.org/10.1038/nature26147.

Brookes, M.J., Groom, M.J., Liuzzi, L., Hill, R.M., Smith, H.J.F., Briley, P.M., Hall, E.L., Hunt, B.A.E., Gascoyne, L.E., Taylor, M.J., Liddle, P.F., Morris, P.G., Woolrich, M.W., Liddle, E.B., 2018. Altered temporal stability in dynamic neural networks underlies connectivity changes in neurodevelopment. Neuroimage 174, 563–575. https://doi.org/10.1016/j.neuroimage.2018.03.008.

Brookes, M.J., Woolrich, M., Luckhoo, H., Price, D., Hale, J.R., Stephenson, M.C., Barnes, G.R., Smith, S.M., Morris, P.G., 2011. Investigating the electrophysiological basis of resting state networks using magnetoencephalography. Proc. Natl. Acad. Sci. U.S.A. 108, 16783–16788. https://doi.org/10.1073/pnas.1112685108.

Brookes, M.J., Woolrich, M.W., Barnes, G.R., 2012. Measuring functional connectivity in MEG: a multivariate approach insensitive to linear source leakage. Neuroimage 63, 910–920. https://doi.org/10.1016/j.neuroimage.2012.03.048.

Colclough, G.L., Brookes, M.J., Smith, S.M., Woolrich, M.W., 2015. A symmetric multivariate leakage correction for MEG connectomes. Neuroimage 117, 439–448. https://doi.org/10.1016/j.neuroimage.2015.03.071.

Coquelet, N., Mary, A., Peigneux, P., Goldman, S., Wens, V., De Tiège, X., 2017. The electrophysiological connectome is maintained in healthy elders: a power envelope correlation MEG study. Sci. Rep. 7, 13984. https://doi.org/10.1038/s41598-017-13829-8.

Craddock, R.C., Tungaraza, R.L., Milham, M.P., 2015. Connectomics and new approaches for analyzing human brain functional connectivity. GigaScience 4, 13. https://doi.org/10.1186/s13742-015-0045-x.

Dale, A.M., Sereno, M.I., 1993. Improved localization of cortical activity by combining EEG and MEG with MRI cortical surface reconstruction: a linear approach. J. Cogn. Neurosci. 5, 162–176. https://doi.org/10.1162/jocn.1993.5.2.162.

Damaraju, E., Allen, E.A., Belger, A., Ford, J.M., McEwen, S., Mathalon, D.H., Mueller, B.A., Pearlson, G.D., Potkin, S.G., Preda, A., Turner, J.A., Vaidya, J.G., van Erp, T.G., Calhoun, V.D., 2014. Dynamic functional connectivity analysis reveals transient states of dysconnectivity in schizophrenia. Neuroimage Clin 5, 298–308. https://doi.org/10.1016/j.nicl.2014.07.003.

de Pasquale, F., Corbetta, M., Betti, V., Della Penna, S., 2018. Cortical cores in network dynamics. Neuroimage 180, 370–382. https://doi.org/10.1016/j.neuroimage.2017.09.063.

de Pasquale, F., Della Penna, S., Snyder, A.Z., Lewis, C., Mantini, D., Marzetti, L., Belardinelli, P., Ciancetta, L., Pizzella, V., Romani, G.L., Corbetta, M., 2010. Temporal dynamics of spontaneous MEG activity in brain networks. Proc. Natl. Acad. Sci. U.S.A. 107, 6040–6045. https://doi.org/10.1073/pnas.0913863107.

de Pasquale, F., Della Penna, S., Snyder, A.Z., Marzetti, L., Pizzella, V., Romani, G.L., Corbetta, M., 2012. A cortical core for dynamic integration of functional networks in the resting human brain. Neuron 74, 753–764. https://doi.org/10.1016/j.neuron.2012.03.031.

de Pasquale, F., Della Penna, S., Sporns, O., Romani, G.L., Corbetta, M., 2016. A dynamic core network and global efficiency in the resting human brain. Cerebr. Cortex 26, 4015–4033. https://doi.org/10.1093/cercor/bhv185.

De Tiège, X., Op de Beeck, M., Funke, M., Legros, B., Parkkonen, L., Goldman, S., Van Bogaert, P., 2008. Recording epileptic activity with MEG in a light-weight magnetic shield. Epilepsy Res. 82, 227–231. https://doi.org/10.1016/j.eplepsyres.2008.08.011.

Deco, G., Corbetta, M., 2011. The dynamical balance of the brain at rest. The Neuroscientist 17, 107–123. https://doi.org/10.1177/1073858409354384.

D'Esposito, M., Deouell, L.Y., Gazzaley, A., 2003. Alterations in the BOLD fMRI signal with ageing and disease: a challenge for neuroimaging. Nat. Rev. Neurosci. 4, 863–872. https://doi.org/10.1038/nrn1246.

Fox, M.D., 2018. Mapping symptoms to brain networks with the human connectome. N. Engl. J. Med. 379, 2237–2245. https://doi.org/10.1056/NEJMra1706158.

Fox, M.D., Greicius, M., 2010. Clinical applications of resting state functional connectivity. Front. Syst. Neurosci. 4, 19. https://doi.org/10.3389/fnsys.2010.00019.

Fox, M.D., Raichle, M.E., 2007. Spontaneous fluctuations in brain activity observed with functional magnetic resonance imaging. Nat. Rev. Neurosci. 8, 700–711. https://doi.org/10.1038/nrn2201.

Friston, K.J., 2011. Functional and effective connectivity: a review. Brain Connect. 1, 13–36. https://doi.org/10.1089/brain.2011.0008.

Gençer, N.G., Acar, C.E., 2004. Sensitivity of EEG and MEG measurements to tissue conductivity. Phys. Med. Biol. 49, 701–717.

Harri, R., Puce, A., 2017. MEG-EEG Primer. Oxford University Press, Oxford, New York.

Hipp, J.F., Hawellek, D.J., Corbetta, M., Siegel, M., Engel, A.K., 2012. Large-scale cortical correlation structure of spontaneous oscillatory activity. Nat. Neurosci. 15, 884–890. https://doi.org/10.1038/nn.3101.

Hutchison, R.M., Womelsdorf, T., Allen, E.A., Bandettini, P.A., Calhoun, V.D., Corbetta, M., Della Penna, S., Duyn, J.H., Glover, G.H., Gonzalez-Castillo, J., Handwerker, D.A., Keilholz, S., Kiviniemi, V., Leopold, D.A., de Pasquale, F., Sporns, O., Walter, M., Chang, C., 2013. Dynamic functional connectivity: promise, issues, and interpretations. Neuroimage 80, 360–378. https://doi.org/10.1016/j.neuroimage.2013.05.079.

Kiebel, S.J., Holmes, C., 2007. The General Linear Model. In: Friston, K., Ashburner, J., Kiebel, S., Nichols, T., Penny, W. (Eds.), Statistical Parametric Mapping: The Analysis of Functional Brain Images. Academic Press, pp. 101–125.

Knyazev, G.G., Savostyanov, A.N., Bocharov, A.V., Tamozhnikov, S.S., Saprigyn, A.E., 2016. Task-positive and task-negative networks and their relation to depression: EEG beamformer analysis. Behav. Brain Res. 306, 160–169. https://doi.org/10.1016/j.bbr.2016.03.033.

Leech, R., Sharp, D.J., 2014. The role of the posterior cingulate cortex in cognition and disease. Brain 137, 12–32. https://doi.org/10.1093/brain/awt162.

Liu, A.K., Dale, A.M., Belliveau, J.W., 2002. Monte Carlo simulation studies of EEG and MEG localization accuracy. Hum. Brain Mapp. 16, 47–62.

Liu, Q., Farahibozorg, S., Porcaro, C., Wenderoth, N., Mantini, D., 2017. Detecting large-scale networks in the human brain using high-density electroencephalography. Hum. Brain Mapp. 38, 4631–4643. https://doi.org/10.1002/hbm.23688.

Liu, Q., Ganzetti, M., Wenderoth, N., Mantini, D., 2018. Detecting large-scale brain networks using EEG: impact of electrode density, head modeling and source localization. Front. Neuroinf. 12, 4. https://doi.org/10.3389/fninf.2018.00004.

Liuzzi, L., Gascoyne, L.E., Tewarie, P.K., Barratt, E.L., Boto, E., Brookes, M.J., 2017. Optimising experimental design for MEG resting state functional connectivity measurement. Neuroimage 155, 565–576. https://doi.org/10.1016/j.neuroimage.2016.11.064.

Lloyd, S., 1982. Least squares quantization in PCM. IEEE Trans. Inf. Theory 28, 129–137. https://doi.org/10.1109/TIT.1982.1056489.

Marty, B., Naeije, G., Bourguignon, M., Wens, V., Jousmäki, V., Lynch, D.R., Gaetz, W., Goldman, S., Hari, R., Pandolfo, M., De Tiège, X., 2019. Evidence for genetically determined degeneration of proprioceptive tracts in Friedreich ataxia. Neurology 93, e116–e124. https://doi.org/10.1212/WNL.0000000000007750.

Naeije, G., Wens, V., Bourguignon, M., Goldman, S., Pandolfo, M., De Tiège, X., 2019. Altered neocortical tactile but preserved auditory early change detection responses in Friedreich ataxia. Clin. Neurophysiol. 130, 1299–1310. https://doi.org/10.1016/j.clinph.2019.05.003.

Nichols, T.E., Holmes, A.P., 2002. Nonparametric permutation tests for functional neuroimaging: a primer with examples. Hum. Brain Mapp. 15, 1–25.

Oldfield, R.C., 1971. The assessment and analysis of handedness: the Edinburgh inventory. Neuropsychologia 9, 97–113.

O'Neill, G.C., Barratt, E.L., Hunt, B.A.E., Tewarie, P.K., Brookes, M.J., 2015a. Measuring electrophysiological connectivity by power envelope correlation: a technical review on MEG methods. Phys. Med. Biol. 60, R271–R295. https://doi.org/10.1088/0031-9155/60/21/R271.

O'Neill, G.C., Bauer, M., Woolrich, M.W., Morris, P.G., Barnes, G.R., Brookes, M.J., 2015b. Dynamic recruitment of resting state sub-networks. Neuroimage 115, 85–95. https://doi.org/10.1016/j.neuroimage.2015.04.030.

O'Neill, G.C., Tewarie, P., Vidaurre, D., Liuzzi, L., Woolrich, M.W., Brookes, M.J., 2018. Dynamics of large-scale electrophysiological networks: a technical review. Neuroimage 180, 559–576. https://doi.org/10.1016/j.neuroimage.2017.10.003.

Palva, J.M., Wang, S.H., Palva, S., Zhigalov, A., Monto, S., Brookes, M.J., Schoffelen, J.-M., Jerbi, K., 2018. Ghost interactions in MEG/EEG source space: a note of caution on inter-areal coupling measures. Neuroimage 173, 632–643. https://doi.org/10.1016/j.neuroimage.2018.02.032.

Pascual-Marqui, R.D., 2002. Standardized low-resolution brain electromagnetic tomography (sLORETA): technical details. Methods Find. Exp. Clin. Pharmacol. 24 (Suppl. D), 5–12.

Perrin, F., Pernier, J., Bertrand, O., Echallier, J.F., 1989. Spherical splines for scalp potential and current density mapping. Electroencephalogr. Clin. Neurophysiol. 72, 184–187.

Siems, M., Pape, A.-A., Hipp, J.F., Siegel, M., 2016. Measuring the cortical correlation structure of spontaneous oscillatory activity with EEG and MEG. Neuroimage 129, 345–355. https://doi.org/10.1016/j.neuroimage.2016.01.055.

Sjøgård, M., De Tiège, X., Mary, A., Peigneux, P., Goldman, S., Nagels, G., van Schependom, J., Quinn, A.J., Woolrich, M.W., Wens, V., 2019. Do the posterior midline cortices belong to the electrophysiological default-mode network? Neuroimage 200, 221–230. https://doi.org/10.1016/j.neuroimage.2019.06.052.

Sockeel, S., Schwartz, D., Pélégrini-Issac, M., Benali, H., 2016. Large-scale functional networks identified from resting-state EEG using spatial ICA. PLoS One 11, e0146845. https://doi.org/10.1371/journal.pone.0146845.

Taulu, S., Simola, J., Kajola, M., 2005. Applications of the signal space separation method. IEEE Trans. Signal Process. 53, 3359–3372. https://doi.org/10.1109/TSP.2005.853302.

Tzourio-Mazoyer, N., Landeau, B., Papathanassiou, D., Crivello, F., Etard, O., Delcroix, N., Mazoyer, B., Joliot, M., 2002. Automated anatomical labeling of activations in SPM using a macroscopic anatomical parcellation of the MNI MRI single-subject brain. Neuroimage 15, 273–289. https://doi.org/10.1006/nimg.2001.0978.

Vidaurre, D., Hunt, L.T., Quinn, A.J., Hunt, B.A.E., Brookes, M.J., Nobre, A.C., Woolrich, M.W., 2018. Spontaneous cortical activity transiently organises into frequency specific phase-coupling networks. Nat Comm 9, 2987. https://doi.org/10.1038/s41467-018-05316-z.

Vigário, R., Särelä, J., Jousmäki, V., Hämäläinen, M., Oja, E., 2000. Independent component approach to the analysis of EEG and MEG recordings. IEEE Trans. Biomed. Eng. 47, 589–593. https://doi.org/10.1109/10.841330.

Vorwerk, J., Oostenveld, R., Piastra, M.C., Magyari, L., Wolters, C.H., 2018. The FieldTrip-SimBio pipeline for EEG forward solutions. Biomed. Eng. Online 17, 37. https://doi.org/10.1186/s12938-018-0463-y.

Wens, V., Bourguignon, M., Goldman, S., Marty, B., Op de Beeck, M., Clumeck, C., Mary, A., Peigneux, P., Van Bogaert, P., Brookes, M.J., De Tiège, X., 2014a. Inter- and intra-subject variability of neuromagnetic resting state networks. Brain Topogr. 27, 620–634. https://doi.org/10.1007/s10548-014-0364-8.

Wens, V., Bourguignon, M., Vander Ghinst, M., Mary, A., Marty, B., Coquelet, N., Naeije, G., Peigneux, P., Goldman, S., De Tiège, X., 2019. Synchrony, metastability, dynamic integration, and competition in the spontaneous functional connectivity of the human brain. Neuroimage. https://doi.org/10.1016/j.neuroimage.2019.05.081.

Wens, V., Marty, B., Mary, A., Bourguignon, M., Op de Beeck, M., Goldman, S., Van Bogaert, P., Peigneux, P., De Tiège, X., 2015. A geometric correction scheme for spatial leakage effects in MEG/EEG seed-based functional connectivity mapping. Hum. Brain Mapp. 36, 4604–4621. https://doi.org/10.1002/hbm.22943.

Wens, V., Mary, A., Bourguignon, M., Goldman, S., Marty, B., Op de Beeck, M., Bogaert, P.V., Peigneux, P., De Tiège, X., 2014b. About the electrophysiological basis of resting state networks. Clin. Neurophysiol. 125, 1711–1713. https://doi.org/10.1016/j.clinph.2013.11.039.

Wolters, C.H., Anwander, A., Tricoche, X., Weinstein, D., Koch, M.A., MacLeod, R.S., 2006. Influence of tissue conductivity anisotropy on EEG/MEG field and return current computation in a realistic head model: a simulation and visualization study using high-resolution finite element modeling. Neuroimage 30, 813–826. https://doi.org/10.1016/j.neuroimage.2005.10.014.

Xia, M., Wang, J., He, Y., 2013. BrainNet Viewer: a network visualization tool for human brain connectomics. PLoS One 8, e68910. https://doi.org/10.1371/journal.pone.0068910.